

<https://doi.org/10.15407/ujpe69.10.719>

I. OTETE,¹ OMAMOKE O.E. ENAROSEHA,² S.I. OKUNZUWA,³ A.I.I. EJERE³

¹ Department of Physics, Federal University
(Otuoke, Nigeria)

² Department of Physics, Faculty of Sciences, Delta State University
(Abraka, Nigeria; e-mail: enarosehaomamoke@gmail.com)

³ Department of Physics, Faculty of Physical Sciences, University of Benin
(Benin City, Nigeria)

SPECTRA AND THERMODYNAMIC PROPERTIES OF ZIG-ZAG SINGLE – WALLED CARBON NANOTUBES WITH DENG–FAN–HULTHEN POTENTIAL

A theoretical investigation of the spectra and thermodynamic properties of zig-zag single-walled carbon nanotubes (6,0) is carried out within the framework of the Deng–Fan–Hulthen potential. We solved the Schrödinger wave equation analytically in the presence of magnetic and Aharonov–Bohm (AB) flux fields using the Nikiforov–Uvarov (NU) method and obtained the energy eigenvalues and eigenfunctions. It is observed that, in the absence of both magnetic and AB fields, there is a degeneracy in the energy spectra. The presence of the magnetic and AB flux fields led to an increase in the energy eigenvalues. The combined presence of both fields removed the degeneracy noticed in the system. We calculated the partition function and used it to evaluate the thermodynamic properties such as the mean energy, free energy, and entropy in respect to the temperature, magnetic field, AB flux field and the quantum numbers.

Keywords: Deng–Fan–Hulthen potential, magnetic field, Aharonov–Bohm flux field, Nikiforov–Uvarov method.

1. Introduction

Carbon nanotubes (CNTs) are sheets of graphene rolled around a central axis, forming the hollow cylindrical shape. CNTs are in two types—single-walled nanotubes (SWNTs) and Multi-walled nanotubes (MWNTs). CNT comprises of a network of carbon atoms in hexagonal form. Their diameter is in the neighborhood of 1 and 2 nanometers, while their length is equal to several micrometers [1]. Due to the small nanoscale diameter, the confinement and movement of electrons are along their length. Hence, CNTs are regarded as 1D nanomaterials [2].

CNTs can be synthesized by various methods which include the arc-discharge, laser ablation, chemical va-

por deposition, plasma and floating catalyst methods [3]. The unique electronic, al, and high thermal conductivity among others that CNTs exhibit have made them research hub for unravelling the fundamental physics in low dimensional systems by physicists and material scientists in [4, 5]. Due to the growing advances in the world of namechanie, CNTs are on the edge of intense research to fully harness their full potential and technological applications. Concerted effort and means are being deployed to investigate their structure and their different properties to unveil the novelty of this material. For instance, molecular dynamics (MD) simulations have been used in the theoretical investigations of the mechanical properties and some thermal properties of CNTs with some empirical potentials like Tersoff, Brenner, Morse, and Lennard-Jones ones. These potentials give description of the potential energy of interaction that exists between two non-bonding atoms or molecules. They serve as a model of interatomic interaction between an atom and the surface. First-principles methods have also been used for the electronic and mechanical

Citation: Otete I., Enaroseha Omamoke O.E., Okunzuwa S.I., Ejere A.I.I. Spectra and thermodynamic properties of zig-zag single – walled carbon nanotube with Deng–Fan–Hulthen potential. *Ukr. J. Phys.* **69**, No. 10, 719 (2024). <https://doi.org/10.15407/ujpe69.10.719>.

© Publisher PH “Akademperiodyka” of the NAS of Ukraine, 2024. This is an open access article under the CC BY-NC-ND license (<https://creativecommons.org/licenses/by-nc-nd/4.0/>)

ISSN 2071-0194. *Ukr. J. Phys.* 2024. Vol. 69, No. 10

properties of CNTs. Experimentally, atomic force microscopy (AFM) has been used to study the mechanical properties of CNTs. For heat or thermal transport in nanotubes, the Boltzmann transport techniques is used [6–9]. Experimental work has also been done in terms of the optical properties of CNTs. Photoluminescence excitation (PLE) spectroscopy, Raman spectroscopy, ultrafast optical spectroscopy, micro- and nanospectroscopies and magneto-optical spectroscopy are some of the optical techniques employed to explore the intrinsic optical properties of CNTs [10].

In this work, the Deng–Fan–Hulthen potential will be used. It is a combination of two different potentials, Deng–Fan and Hulthen potentials. Deng–Fan potential was proposed in 1957 to study molecular systems. It is one of the exponential potentials that is consistent with quantum criteria. It is a veritable tool to study physical systems by theoretical physicists, and a Pekeris-type approximation is usually employed to handle the centrifugal term [11]. It is regarded as one of the simplest modified Morse potentials. Under the boundary condition $r = 0 \wedge \infty$, the Deng–Fan potential behaves itself correctly [12]. The Hulthen potential has always played a pivotal role in condense matter physics, atomic physics, nuclear physics, and solid-state physics. It has been used to describe the molecular structure of an atom and nuclear interaction. It is a short-range potential that exhibits a Coulomb-like behavior for small values of the screening parameter r with an exponential decrease for large values of r [13–15].

The organization of this paper is as follows; in Section 2, we will consider the quantum Hamiltonian of a charged particle confined in a region of potential in the presence of magnetic field and Aharonov–Bohm (AB) flux and solve analytically the radial part of the Schrödinger equation with the NU method to obtain the energy eigenvalues and the wave function. We present numerical results and graphical plots in Section 3. In Section 4, we determine the partition function and thermodynamic properties of zig-zag single-walled carbon nanotubes (6, 0). The discussion of our results is done in Section 5, while our conclusions will be given in the last section.

2. Theoretical Model and Formulation

The quantum Hamiltonian of a charged particle confined in a region of potential (Deng–Fan–Hulthen po-

tential) under the combined influence of an external magnetic field B and Aharonov–Bohm (AB) flux in the cylindrical coordinate is written as

$$\frac{1}{2\mu} \left(\mathbf{p} - \frac{e}{c} \mathbf{A} \right)^2 + D_e \left(1 - \frac{\Omega}{(e^{\delta r} - 1)} \right)^2 - \frac{V_0 e^{\delta r}}{(1 - e^{-\delta r})} = E_{(n,m)} \psi_{(\rho,\varphi,z)}, \quad (1)$$

where $\Omega = e^{\delta r_e} - 1$, D_e is the dissociation energy, r_e is the molecular bond length, r is the internuclear distance, δ is the range of the potential well, and V_0 is the potential strength [16].

Here, we take μ to be the effective mass for CNT. The vector potential \mathbf{A} is written as the sum of two terms, $\mathbf{A} = \mathbf{A}_1 + \mathbf{A}_2$, and our symmetric or Coulomb gauge is written as $\nabla \times \mathbf{A}_1 = \mathbf{B}$ and $\nabla \times \mathbf{A}_2 = 0$, where B_z represents the applied magnetic field along the Z -axis. The additional magnetic flux Φ_{AB} is due to a solenoid. Thus, in the cylindrical coordinate system, the vector potential has the azimuthal components

$$\mathbf{A}_1 = \frac{\mathbf{B} e^{-\delta r}}{(1 - e^{-\delta r})}, \quad \mathbf{A}_2 = \frac{\Phi_{AB}}{2\pi r}, \quad (2)$$

$$\mathbf{A} = \left(0, \frac{\mathbf{B} e^{-\delta r}}{(1 - e^{-\delta r})} + \frac{\Phi_{AB}}{2\pi r}, 0 \right)$$

[17]. The Deng–Fan–Hulthen Potential which is our confining potential is a combination of two different potentials – Deng–Fan and Hulthen potentials.

We take a wave function in the cylindrical coordinates as

$$\psi_{(r,\varphi)} = \frac{1}{\sqrt{2\pi}} e^{im\varphi} R_{nm}(r), \quad m = 0, \pm 1, \pm 2 \dots, \quad (3)$$

where m represents the magnetic quantum number. By inserting our confining potential, vector potential, and the wave function into Eq. (1), a second-order differential equation will be obtained:

$$\frac{d^2 R_{nm}(r)}{dr^2} + \frac{2\mu}{\hbar^2} \left[E - D_e^2 + \frac{V_0 e^{-\delta r}}{(1 - e^{-\delta r})} - \frac{2\hbar m e \delta \mathbf{B} e^{-\delta r}}{c(1 - e^{-\delta r})} - \frac{e^2 \mathbf{B} e^{-2\delta r}}{c^2} \right] R_{nm}(r) = 0. \quad (4)$$

Since this differential equation contains both exponential and radial terms, the improved approximation

scheme by Greene and Aldrich given in the equation below will help to solve the equation [17]

$$\frac{1}{r^2} \approx \delta^2 \left[d_o + \frac{e^{-\delta r}}{(1 - e^{-\delta r})} \right]^2. \quad (5)$$

By inserting Eq. (5) into Eq. (4), we have

$$\begin{aligned} \frac{d^2 R_{nm}(r)}{dr^2} + \left[\frac{2\mu E}{\hbar^2} - \frac{2\mu D_e}{\hbar^2} + \frac{4\mu D_e \Omega e^{-\delta r}}{\hbar^2 (1 - e^{-\delta r})} - \frac{2D_e \Omega^2 e^{-2\delta r}}{\hbar^2 (1 - e^{-\delta r})^2} + \frac{2V_0 e^{-\delta r}}{\hbar^2 (1 - e^{-\delta r})} - \frac{2m\eta \delta \mathbf{B} e^{-\delta r}}{\hbar^2 (1 - e^{-\delta r})^2} - \frac{\eta^2 \mathbf{B}^2 e^{-2\delta r}}{\hbar^2 (1 - e^{-\delta r})^2} - \frac{\eta^2 \delta \mathbf{B} \Phi_{AB} e^{-\delta r}}{\hbar^2 (1 - e^{-\delta r})^2} \pi - \left((m + \zeta) - \frac{1}{4} \right) \delta^2 \left(d_o + \frac{e^{-\delta r}}{(1 - e^{-\delta r})} \right)^2 \right] R_{nm}(r) = 0, \quad (6) \end{aligned}$$

where $\eta = \frac{e}{c}$, $\Phi_0 = \frac{\hbar c}{e}$, $\zeta = \frac{\Phi_{AB}}{\Phi_0}$ and $\Omega = e^{\delta r} - 1$, c is the speed of light.

Let us use the transformation

$$s = e^{-\delta r}. \quad (7)$$

After differentiating twice, we obtain

$$\frac{d^2}{ds^2} = \frac{\delta^2 s^2 d^2}{ds^2} + \frac{\delta^2 s d}{ds}. \quad (8)$$

Substituting Eq. (8) into Eq. (6) and dividing by $\delta^2 S^2$, we get:

$$\begin{aligned} \frac{d^2 R}{ds^2} + \frac{1}{S} \frac{dR}{ds} + \frac{1}{S^2} \left[\frac{2\mu E}{\hbar^2 \delta^2} - \frac{2\mu D_e}{\hbar^2 \delta^2} + \frac{4\mu D_e \Omega S}{\hbar^2 \delta^2 (1 - S)} - \frac{2\mu D_e \Omega^2 S^2}{\hbar^2 \delta^2} + \frac{2\mu V_0 S}{\hbar^2 \delta^2 (1 - S)} - \frac{2m\eta \mathbf{B} S}{\hbar \delta (1 - S)^2} - \frac{\eta^2 \mathbf{B}^2 S^2}{\hbar^2 \delta^2 (1 - S)^2} \right] \frac{-\eta^2 \mathbf{B} \Phi_{AB} S}{\hbar^2 \delta (1 - S)^2 \pi} = 0. \quad (9) \end{aligned}$$

The following dimensionless symbols were used for mathematical convenience

$$\begin{aligned} -\varepsilon &= \frac{2\mu(E_{nm} - D_e)}{\hbar^2 \delta^2}, \quad \beta_1 = \frac{4\mu D_e \Omega}{\hbar^2 \delta^2}, \quad \beta_2 = \frac{2\mu D_e \Omega^2}{\hbar^2 \delta^2}, \\ \rho &= \frac{2\mu V_0}{\hbar^2 \delta^2}, \quad \chi = \frac{2m\eta \mathbf{B}}{\hbar \delta}, \quad \lambda_1 = \frac{\eta^2 \mathbf{B}^2}{\hbar^2 \delta^2}, \quad (10) \\ \lambda_2 &= \frac{\eta^2 \mathbf{B} \Phi_{AB}}{\hbar^2 \delta^2 \pi}, \quad V = \left((m + \zeta)^2 - \frac{1}{4} \right). \end{aligned}$$

Equation (9) can be rewritten with respect to these dimensionless symbols as

$$\begin{aligned} \frac{d^2 R}{ds^2} + \frac{(1 - S)}{S(1 - S)} \frac{dR}{ds} + \frac{1}{S^2 (1 - S)^2} (1 - S)^2 + \\ + \beta_1 (1 - S) S - \beta_2 (S^2) + \rho (1 - S) S - \chi(S) - \lambda_1 (S^2) - \\ - \lambda_2 (1 - S) S - V d_o (1 - S)^2 = 0. \quad (11) \end{aligned}$$

Subsequently, Eq. (11) can be evaluated further as

$$\begin{aligned} \frac{d^2 R}{ds^2} + \frac{(1 - S)}{S(1 - S)} \frac{dR}{ds} + \frac{1}{S^2 (1 - S)^2} \times \\ \times [-(\varepsilon + \beta_1 + \beta_1 + \rho + \lambda_1 - \lambda_2 + V d_o) S^2 + \\ + (2\varepsilon + \beta_1 + \rho - \chi - \lambda_2 + 2V d_o - V) S - \\ - (\varepsilon + V d_o)] R_{nm} = 0. \quad (12) \end{aligned}$$

Equation (12) is compared with the parametric NU form of Eq. (13) written as [18]

$$\begin{aligned} R'' + \frac{\delta_1 - \delta_2 S}{S(1 - \delta_3 S)} R' + \\ + \left[\frac{-\xi_1 S^2 + \xi_2 S - \xi_3}{S^2 (1 - \delta_3 S)^2} \right] R_{(s)} = 0. \quad (13) \end{aligned}$$

The equation for energy eigenvalues, according to the NU method, is written as

$$\begin{aligned} \delta_2 n - (2n + 1) \delta_5 + (2n + 1) [\sqrt{\delta_9} + \delta_3 \sqrt{\delta_8}] + \\ + n(n - 1) \delta_3 + \delta_7 + 2\delta_3 \delta_8 + 2\sqrt{\delta_8 \delta_9} = 0. \quad (14) \end{aligned}$$

The corresponding wave function is given as

$$\begin{aligned} R_{nm}(s) = s^{\delta_{12}} (1 - \delta_3 s)^{-\delta_{12} - \delta_{13}/\delta_3} \times \\ \times p_n^{(\delta_{10}-1)\left(\frac{\delta_{11}}{\delta_3}\right) - (\delta_{10}-1)} (1 - 2\delta_3 s), \quad (15) \end{aligned}$$

where the following parameters are used:

$$\delta_4 = \frac{1}{2} (1 - \delta_1), \quad (16)$$

$$\delta_5 = \frac{1}{2} (\delta_2 - 2\delta_3), \quad (17)$$

$$\delta_6 = \delta_5 + \xi_1, \quad (18)$$

$$\delta_7 = 2\delta_4 \delta_5 - \xi_2, \quad (19)$$

$$\delta_8 = \delta_4^2 + \xi_3, \quad (20)$$

$$\delta_9 = \delta_3 \delta_7 + \delta_3^2 \delta_8 + \delta_6, \quad (21)$$

$$\delta_{10} = \delta_1 + 2\delta_4 + 2\sqrt{\delta_8}, \tag{22}$$

$$\delta_{11} = \delta_2 - 2\delta_5 + 2\left(\sqrt{\delta_9} + \delta_3\sqrt{\delta_8}\right), \tag{23}$$

$$\delta_{12} = \delta_4 + \sqrt{\delta_8}, \tag{24}$$

$$\delta_{13} = \delta_5 - \left(\sqrt{\delta_9} + \delta_3\sqrt{\delta_8}\right). \tag{25}$$

When Eq. (12) is compared with the parametric NU form Eq. (13). The following parameters can be introduced:

$$\delta_1 = \delta_2 = \delta_3 = 1, \tag{26}$$

$$\xi_1 = \varepsilon + \beta_1 + \beta_1 + \rho + \lambda_1 - \lambda_2 + Vd_0, \tag{27}$$

$$\xi_2 = 2\varepsilon + \beta_1 + \rho - \chi - \lambda_2 + 2Vd_0 - V, \tag{28}$$

$$\xi_3 = \varepsilon + Vd_0. \tag{29}$$

From Eqs. (16)–(21) we obtain

$$\delta_4 = \frac{1}{2}(1 - \delta_1) = 0, \quad \delta_5 = \frac{1}{2}(\delta_2 - 2\delta_3) = -\frac{1}{2}, \tag{30}$$

$$\delta_6 = \delta_5^2 + \xi_1 = \frac{1}{4} + \varepsilon + \beta_1 + \beta_1 + \rho + \lambda_1 - \lambda_2 + Vd_0, \tag{30}$$

$$\delta_7 = 2\delta_4\delta_5 - \xi_2 = - (2\varepsilon + \beta_1 + \rho - \chi - \lambda_2 + 2Vd_0 - V), \tag{31}$$

$$\delta_8 = \delta_4^2 + \xi_3 = \varepsilon + Vd_0 \tag{32}$$

$$\delta_9 = \delta_3\delta_7 + \delta_3^2\delta_8 + \delta_6 = \frac{1}{4} + \chi + V + \lambda_1 + \beta_2. \tag{33}$$

Recall that, in Eq. (10),

$$-\varepsilon = \frac{2\mu(E_{nm} - D_e)}{\hbar^2\delta^2}. \tag{34}$$

So, substituting Eqs. (30)–(33) into Eq. (14) and carrying out some algebra, we get the equation for energy eigenvalue with the Deng–Fan–Hulthen potential as:

$$E_{nm} = \frac{-\hbar^2\delta^2}{2\mu}, \tag{35}$$

where

$$\begin{aligned} \sigma &= \frac{1}{4} + \chi + V + \lambda_1 + \beta_2\Lambda = \\ &= -\beta_1 - \rho + \chi + \lambda_2 + V\tau = n + \frac{1}{2}. \end{aligned} \tag{36}$$

Thus, Eq. (36) can be re-written in terms of the dimensionless symbols of Eq. (10) as

$$\sigma = \frac{1}{4} + \frac{2m\eta\mathbf{B}}{\hbar\delta} + (m+\zeta)^2 - \frac{1}{4} + \frac{\eta^2\mathbf{B}^2}{\hbar^2\delta^2} + \frac{2\mu D_e\Omega^2}{\hbar^2\delta^2}, \tag{37}$$

$$\begin{aligned} \Lambda &= \frac{-4\mu D_e\Omega}{\hbar^2\delta^2} - \frac{2\mu V_0}{\hbar^2\delta^2} + \frac{2m\eta\mathbf{B}}{\hbar\delta} + \frac{\eta^2\mathbf{B}\Phi_{AB}}{2\delta\pi} + \\ &+ (m + \zeta)^2 - \frac{1}{4}. \end{aligned} \tag{38}$$

From Eqs. (22)–(25), we determine

$$\delta_{10} = \delta_1 + 2\delta_4 + 2\sqrt{\delta_8} = 1 + 2\sqrt{\varepsilon + Vd_0}, \tag{39}$$

$$\begin{aligned} \delta_{11} &= \delta_2 - 2\delta_5 + 2\left(\sqrt{\delta_9} + \delta_3\sqrt{\delta_8}\right) = 2 + \\ &+ 2\left(\sqrt{\frac{1}{4} + \chi + V + \lambda_1 + \beta_2 + \varepsilon + Vd_0}\right), \end{aligned} \tag{40}$$

$$\delta_{12} = \delta_4 + \sqrt{\delta_8} = \sqrt{\varepsilon + Vd_0}, \tag{41}$$

$$\begin{aligned} \delta_{13} &= \delta_5 - \left(\sqrt{\delta_9} + \delta_3\sqrt{\delta_8}\right) = \\ &= -\frac{1}{2} - \left(\sqrt{\frac{1}{4} + \chi + V + \lambda_1 + \beta_2 + \varepsilon + Vd_0}\right). \end{aligned} \tag{42}$$

Substituting Eqs. (39)–(42) into Eq. (15) we obtain the wave function written in Eq. (43) as

$$\begin{aligned} R_{nm}(s) &= \\ &= s^{\sqrt{\varepsilon+Vd_0}} P_n^{2\sqrt{\varepsilon+Vd_0}, 2\sqrt{\frac{1}{4}+\chi+V+\lambda_1+\beta_2}}(1-2s). \end{aligned} \tag{43}$$

3. Numerical Results and Discussion

With the Maple software, the numerical analysis of the energy spectra is done. For zig-zag SWCNTs (6,0), bond length of 26.480 Å and bond dissociation enthalpy (BDE) also known as dissociation energy to be 4.6761 (eV) were taken in the study [19].

4. Thermodynamic Properties of CNTs

Above, we determined the thermodynamic properties of the system, whose temperature-dependent partition function is first evaluated. At a given temperature, when the direct summation is done over all possible energy levels, the partition function can be evaluated [20]. The partition function is written as

$$Z(\beta) = \sum_n^v e^{-\beta E_{n,m}}, \tag{44}$$

where $\beta = \frac{1}{kT}$ with k is the Boltzmann constant, T the temperature E_{nm} is the energy of the n th bound state, where $n = 0, 1, 2, 3, \dots, n_{\max}$

The energy eigenvalue of Eq. (35) can be re-written as

$$E_{nm} = -\hbar^2 \delta^2, \quad (45)$$

where

$$N_1 = \frac{1}{4} + \frac{2m\eta\mathbf{B}}{\hbar\delta} + (m + \zeta)^2 - \frac{1}{4} + \frac{\eta^2\mathbf{B}^2}{\hbar^2\delta^2} + \frac{2\mu D_e\Omega^2}{\hbar^2\delta^2} + \frac{4\mu D_e\Omega}{\hbar^2\delta^2} - \frac{2\mu V_o}{\hbar^2\delta^2} + \frac{2m\eta\mathbf{B}}{\hbar\delta} + \frac{\eta^2\mathbf{B}\Phi_{AB}}{\hbar^2\delta\pi} + (m + \zeta)^2 - \frac{1}{4}, \quad (46)$$

$$N_2 = \left((m + \zeta)^2 - \frac{1}{4} \right) d_0 \left(\frac{\hbar^2\delta^2}{2\mu} \right) + D_e. \quad (47)$$

Therefore, Eq. (44) can be written as

$$Z_{(\beta)} = \sum_{n=0}^{\nu} e^{-\beta \left[\frac{-\hbar^2\delta^2}{2\mu} \left(\frac{N_1 - (n + \sigma)^2}{2(n + \sigma)} \right)^2 + N_2 \right]}. \quad (48)$$

In the classical limit, the summation of Eq. (48) is replaced by an integral. Therefore, we have

$$Z_{(\beta)} = \int_0^{\nu} e^{(Pl^2\beta + \frac{T\beta}{l^2} + M\beta)} dl, \quad l = n + \sigma, \quad (49)$$

where

$$P = \frac{\hbar^2\delta^2}{8\mu}, \quad T = \frac{-\hbar^2\delta^2 N_1^2}{8\mu}, \quad M = - \left(\frac{\hbar^2\delta^2 N_1}{4\mu} + N_2 \right). \quad (50)$$

The Maple software is used to evaluate Eq. (49) to obtain the partition function of the system:

$$\frac{1}{2} e^{Pl^2\beta + M\beta} \sqrt{-T\beta} \times \left(\frac{2\nu e^{T\beta/\nu^2}}{\sqrt{-T\beta}} - \frac{2\sqrt{T\beta}\sqrt{\pi} \operatorname{erfi} \left(\frac{\sqrt{T\beta}}{\nu} \right)}{\sqrt{-T\beta}} - 2\sqrt{\pi} \right), \quad (51)$$

where $\operatorname{erfi}(k)$ denotes the imaginary error function [21] defined as

$$\operatorname{erfi}(k) = i \operatorname{erf}(k) = \frac{2}{\sqrt{\pi}} \int_0^k e^{t^2} dt. \quad (52)$$

In the Maple software, this error function is used for various numerical calculations.

The plots of the partition function as a function of temperature, magnetic field, AB flux, and ν_{\max} are presented:

Having known the partition function of the system, the thermodynamic properties like the mean energy U , free energy F , and entropy S can be calculated using relations (22)–(23).

Mean the energy

$$U = \frac{-\delta \ln Z}{\delta\beta}. \quad (53)$$

The free energy

$$F = -KT \ln Z, \quad (54)$$

$$S = K \ln Z - \frac{K\beta\delta \ln Z}{\delta\beta}. \quad (55)$$

Tables 1 and 2 show the numerical results of the energy eigenvalues computed with Eq. (35) at two different potential ranges of the potential well, $\delta = 0.02$ and $\delta = 0.2$.

At $\delta = 0.02$, when both the magnetic field and Aharonov Bohm (AB) flux are kept at zero that is, $\mathbf{B} = \zeta = 0$, there is existence of degeneracy in the energy levels for $m = 1, 2$ and $m = -1, -2$. But, when the magnetic field is applied to the system with the AB flux field kept at zero, that is, $\mathbf{B} \neq 0$ $\zeta = 0$, the energy eigenvalues increasingly become more positive in nature as the quantum number n increases for a fixed magnetic quantum number m . The degeneracy noticed in the system was lifted. It is observed that, as the magnetic field increases to $6T$ with AB flux kept at zero, the energy eigenvalues increase and became more positive in nature. When the AB flux is applied and the magnetic field is totally absent, the energy eigenvalues are seen to be more negative for $\mathbf{B} = 0$, $\zeta \neq 0$ compared to $\mathbf{B} \neq 0$, $\zeta = 0$. There was no degeneracy in the system. But, when both fields are present, the energy eigenvalues increase, as they are made more attractive in nature. The combined effect of both fields led to a significant shift in the bound state energy.

At $\delta = 0.2$, when the magnetic field and AB flux are absent, that is, $\mathbf{B} = \zeta = 0$, the system witnessed the degeneracies at the energy levels for $m = 1, 2$ and $m = -1, -2$. The energy eigenvalues became more

Table 1. Energy values for the Deng–Fan–Hulthen model for zig-zag SWCNTC< (6,0) under the influence of magnetic field and AB flux with various n and m states with $\hbar = 1, \mu = 0.046, \delta = 0.02, V_0 = 0.2, r_e = 26.480, D_e = 4.6761$

m	n	$\mathbf{B} = \zeta = 0$	$\mathbf{B} = 2, \zeta = 0$	$\mathbf{B} = 4, \zeta = 0$	$\mathbf{B} = 2, \zeta = 0$	
0	0	-4.587167552	-0.1933532001	-0.02814191252	0.001635647835	
	1	-3.961250136	-0.1335024608	-0.003199210122	0.01532357932	
	2	-3.410336394	-0.08392407285	0.01274548306	0.02022367154	
	3	-2.929031632	-0.04431413608	0.01982512202	0.01642270040	
	1	0	-4.591947204	-0.1347532394	-0.003015603265	0.01564474032
		1	-3.959816268	-0.08487698805	0.01300704036	0.02058340022
		2	-3.409039066	-0.04497792548	0.02016348130	0.01682061789
	-1	3	-2.927851518	-0.01476586900	0.01858347950	0.004441755392
		0	-4.591947204	-0.2618444514	-0.06169284125	-0.02052879601
		1	-3.959816268	-0.1916280366	-0.02765486139	0.002022859352
	2	2	-3.409039066	-0.1319959824	-0.002750577208	0.01569857773
		3	-2.927851518	-0.08262975450	0.01315627138	0.02058657730
0		-4.587167552	-0.08548530250	0.01394066594	0.02166543388	
-2	1	-3.955516780	-0.04521602718	0.02121286008	0.01796679727	
	2	-3.405148902	-0.01464443458	0.01974692462	0.005651454405	
	3	-2.924312739	0.006506782115	0.009669527750	-0.01519661066	
-2	0	-4.587167552	-0.3408292911	-0.10391329832	-0.05101993210	
	1	-3.955516780	-0.2598303065	-0.06061865115	-0.01948754551	
	2	-3.405148902	-0.1897458406	-0.02657773652	0.003079052935	
3	-2.924312739	-0.1302417296	0.001670560252	0.01676956342		
m	n	$\mathbf{B} = 0, \zeta = 2$	$\mathbf{B} = 0, \zeta = 4$	$\mathbf{B} = 0, \zeta = 6$	$\mathbf{B} = \zeta = 6$	
0	0	-4.593541248	-4.587167552	-4.568086061	0.02957662012	
	1	-3.955516780	-3.938350542	-3.909852296	0.01728372806	
	2	-3.405148902	-3.389615508	-3.363822954	-0.003540509548	
	3	-2924312739	-2.910181204	-2.886712039	-0.03281278413	
1	0	-4.515915896	-4.579209722	-4.553813774	0.01340046194	
	1	-3.948358022	-3.925509039	-3.891403094	0.001237174961	
	2	-3.398671358	-3.377993989	-3.347121998	-0.02801170070	
-1	3	-2.918420020	-2.899607222	-2.871512613	-0.06562669445	
	0	-4.553813774	-4.591947204	-4.579209722	0.02926927708	
	1	-3.959816268	-3.948358022	-3.925509039	0.02559484426	
2	2	-3.409039066	-3.398671358	-3.377993989	0.01330424280	
	3	-2.927851518	-2.918420020	-2.899607222	-0.007517727265	
	0	-4.492348170	-4.568086061	-4.536414839	0.006814356365	
-2	1	-3.938350542	-3.909852296	-3.870188115	-0.02238592922	
	2	-3.389615508	-3.363822954	-3.327914075	-0.05995280260	
	3	-2.910181204	-2.886712039	-2.854028801	-0.1058055416	
-2	0	-4.568086061	-4.593541248	-4.587167552	0.02095032174	
	1	-3.961250136	-3.955516780	-3.938350542	0.02600745402	
	2	-3.410336394	-3.405148902	-3.389615508	0.02236190906	
3	-2.929031632	-2.924312739	-2.910181204	0.01009991097		

attractive and increase as the energy levels are increased. But, when the magnetic field is applied, that is, $\mathbf{B} \neq 0, \zeta = 0$, the degeneracies disappears. When

AB flux is applied, that is, $\mathbf{B} = 0, \zeta \neq 0$, the energy eigenvalues appeared more attractive and increase significantly when compared to the case where

Table 2. Energyvalues for the Deng–Fan–Hulthen model for zig-zag SWCNTC< (6,0) under the influence of magnetic field and AB flux with various n and m states with $\hbar = 1, \mu = 0.046, \delta = 0.2, V_0 = 0.2, r_e = 26.480, D_e = 4.6761$

m	n	$\mathbf{B} = \zeta = 0$	$\mathbf{B} = 2, \zeta = 0$	$\mathbf{B} = 4, \zeta = 0$	$\mathbf{B} = 6, \zeta = 0$
0	0	-1.330154556	-1.329221618	-1.326425994	-1.321776289
	1	0.6556819100	0.6562760670	0.6580566835	0.6610172845
	2	1.764839587	1.765097598	1.765870389	1.767153780
1	3	2.001344340	2.001268089	2.001038670	2.000654365
	0	-1.293781866	-1.255710724	-1.216043215	-1.174843726
	1	0.6919981820	0.7162372435	0.7414074370	0.7674562750
-1	2	1.801100012	1.811571406	1.822313450	1.833285277
	3	2.037549042	2.034316206	2.030697256	2.026662887
	0	-1.293781866	-1.330195935	-1.364898246	-1.397838149
-2	1	0.6919981820	0.6687404305	0.6465093510	0.6253482685
	2	1.801100012	1.790938634	1.781124211	1.771691825
	3	2.037549042	2.040424482	2.042970778	2.045215282
-2	0	-1.184664304	-1.109669132	-1.033759775	-0.9570553985
	1	0.8009472855	0.8486182030	0.8965518420	0.9446502770
	2	1.909881130	1.930354530	1.950443288	1.970071444
-2	3	2.146163086	2.139563844	2.131936520	2.123226313
	0	-1.184664304	-1.258628556	-1.331448434	-1.403014388
	1	0.8009472855	0.7536351285	0.7067765830	0.6604635370
-2	2	1.909881130	1.889099400	1.868085280	1.846913788
	3	2.146163086	2.151790515	2.156503492	2.160360226
m	n	$\mathbf{B} = 0, \zeta = 2$	$\mathbf{B} = 0, \zeta = 4$	$\mathbf{B} = 0, \zeta = 6$	$\mathbf{B} = \zeta = 6$
0	0	-1.330154556	-1.184664304	-0.7481941390	0.3118922713
	1	0.8009472855	1.236742760	1.963067920	2.171969180
	2	1.909881130	2.345005344	3.070211340	3.155951154
1	3	2.146163086	2.580619002	3.304711004	3.267856052
	0	0.4520964539	-1.002801210	-0.4208415522	0.8894965225
	1	0.9825290015	1.563589490	2.435178275	2.708432788
-1	2	2.091183076	2.671348320	3.541594439	3.651463206
	3	2.327186408	2.906460558	3.775370087	3.722604046
	0	-0.4208415522	-1.293781866	-1.293781866	-1.949188722
-1	1	0.6919981820	0.9825290015	1.563589490	1.706198322
	2	1.801100012	2.091183076	2.671348320	2.731032256
	3	2.037549042	2.327186408	2.906460558	2.883601946
2	0	-0.2074460913	-0.7481941390	-0.02074460913	1.537879216
	1	1.236742760	1.963067920	2.979920277	3.315574720
	2	2.345005344	3.070211340	4.08549204	4.217553758
-2	3	2.580619002	3.304711004	4.318437508	4.247831061
	0	-0.7481941390	-1.330154556	-1.184664304	-0.6309204005
	1	0.6556819100	0.8009472855	1.236742760	1.311136352
-2	2	1.764839587	1.909881130	2.345005344	2.376721706
	3	2.001344340	2.146163086	2.580619002	2.569856263

$\mathbf{B} \neq 0, \zeta = 0$. When both fields are present, the combined effect of the fields is seen to increase the energy eigenvalues for the quantum levels 0 – 2. It is noticed

that the effect of the AB flux field for $\zeta = 6\mathbf{TB} = 0$ for quantum level $n = 3$ is seen to be stronger than the combine effect, when $\mathbf{B} = \zeta = 6$.

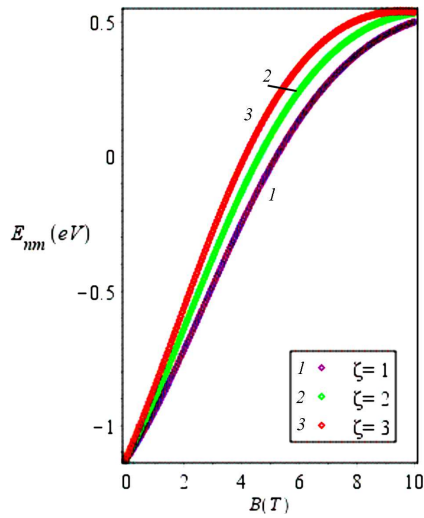


Fig. 1. Plot of the variation of energy, E versus magnetic field B

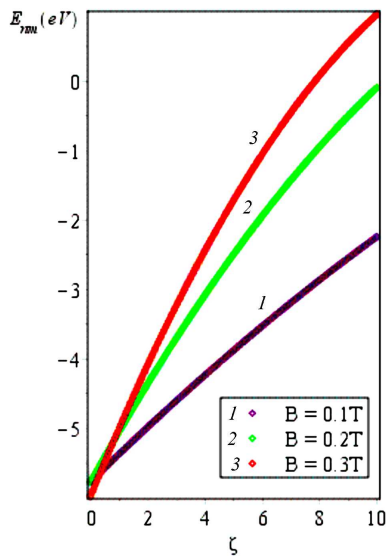


Fig. 2. Plot of energy vs AB flux ζ

So, the adjustment of the potential range $\delta = 0.2$ is seen to bring a significant increase in the energy eigenvalues as the system experienced a noticeable change in the bound state energy than when the potential range, $\delta = 0.02$. Figure 1 depicts the plot of the variation of the energy E with the magnetic field B at various values of the AB flux. It can be seen that the energy eigenvalue increases exponentially as the magnetic field strength increases. Figure 2. Shows the plot of the energy E versus AB flux ζ for different

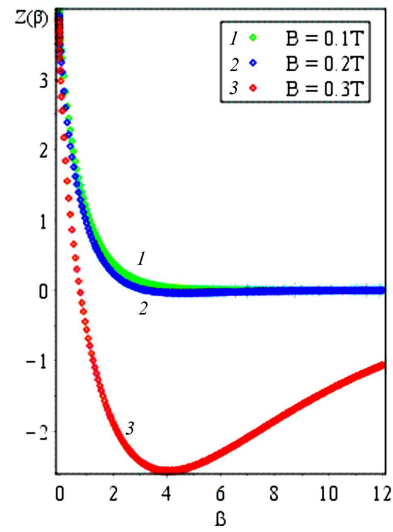


Fig. 3. Plot of partition function versus β for different values of magnetic field

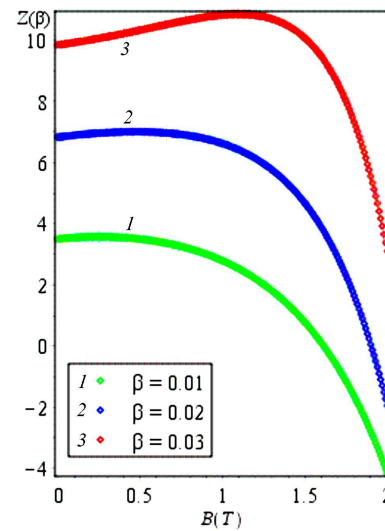


Fig. 4. Plot of partition function versus B for various values of temperature

values of the magnetic field strength. As the AB flux increases, the energy eigenvalues also increase. The results show that if the magnetic field B and AB flux are turn off, the energy eigenvalues can become degenerate in nature. In Fig. 3, we see the behavior of the partition function with varying values of the β for different values of the magnetic field strength. For $B = 0.1T$ and $0.2T$, the partition function decreases in value until when β is about 2.05 K and then becomes invariant. At this point of invariance.

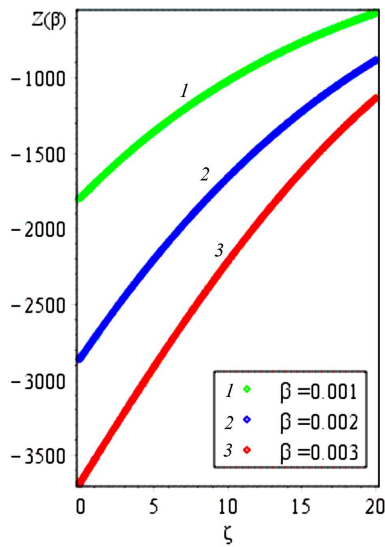


Fig. 5. The plot of partition versus AB flux for various values of temperature

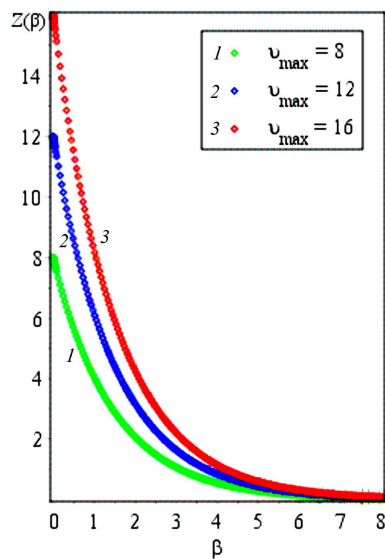


Fig. 6. Plot of partition versus β for various v_{\max}

There is an interaction between the magnetic fields and the partition function, the energy states experience some degree of degeneracy. But, when $B = 0.3T$, it decreases until $\beta \rightarrow 4$, and then increases steadily, when the upper bound quantum number, $v_{\max} = 4$. The influence of the magnetic field has overcome the degeneracy. For Figure 4, the partition function increases exponentially with a decrease in the magnetic field strength with various values of β at different

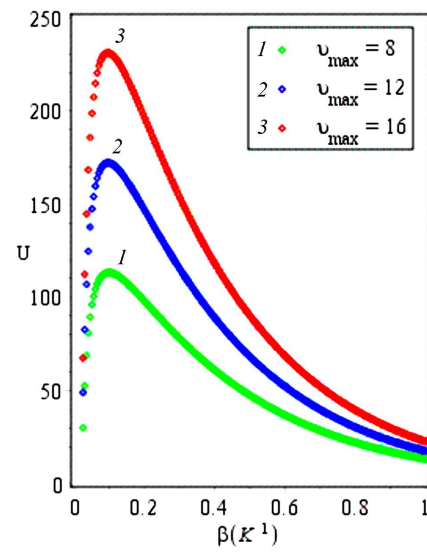


Fig. 7. Plot of mean energy versus temperature for various

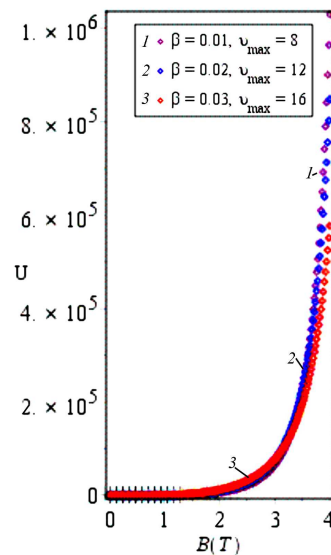


Fig. 8. Plot of mean energy versus magnetic field at various β values and v_{\max}

v_{\max} . Here, the increase in values of the partition function lowers the magnetic field strength. A different behavior of the partition function is observed in Fig. 5 with the AB flux at various values of β . The partition function has negative values that is increasing toward a positive direction with increasing the AB flux field as β is varied gradually upward. The AB flux influence resulted in a much negative values for the partition function. In Fig. 6, the partition func-

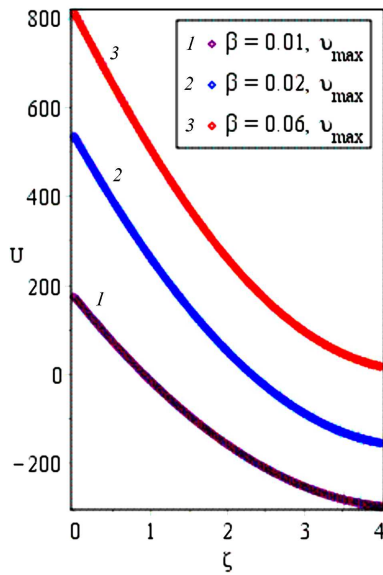


Fig. 9. Plot of mean energy versus AB flux at various v_{\max} and v_{\max}

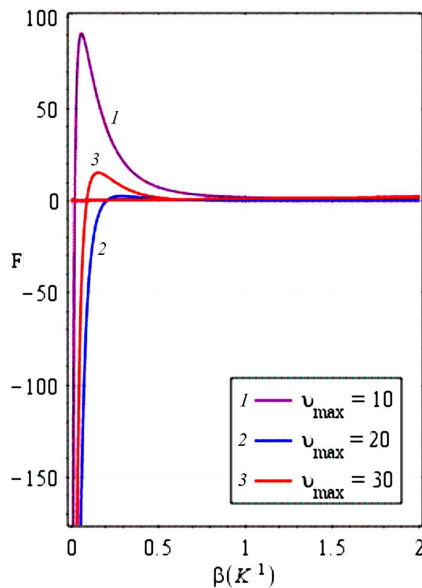


Fig. 10. Plot of free energy versus temperature at various v_{\max}

tion of the system is plotted against β for different v_{\max} . The partition function decreases exponentially with increasing values β for various quantum numbers or energy states. For higher quantum number or energy state s , the Boltzmann factor increases more.

For the mean energy at various v_{\max} in Fig. 7, an initial rise is noticed in the mean energy as the tem-

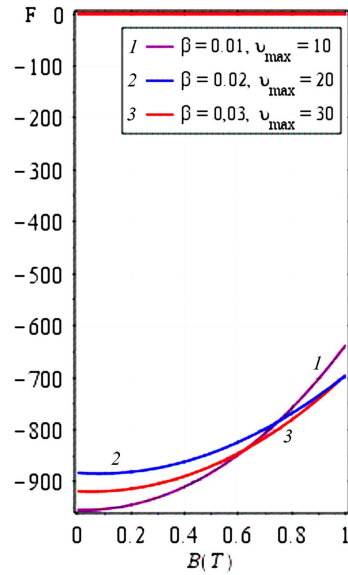


Fig. 11. Plot of free energy versus magnetic field at various temperature and v_{\max}

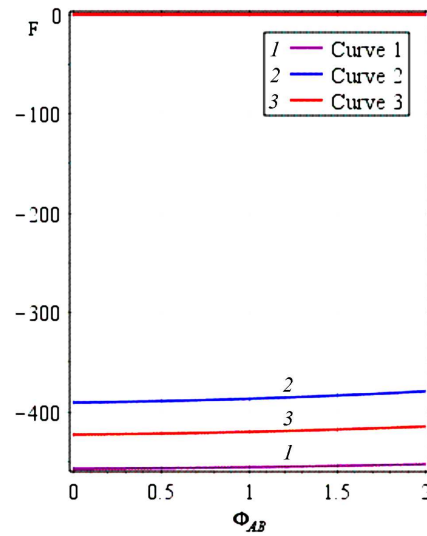


Fig. 12. Plot of free energy versus AB flux at various temperatures and v_{\max}

perature increases. But, the mean energy decreases as the temperature tends to 1. Figure 8 depicts the plot of the mean energy against the magnetic field at various temperatures and v_{\max} . The mean energy increases linearly as the magnetic field strength increases. However, in Fig. 9, the mean energy plot against the AB flux at various temperatures and v_{\max}

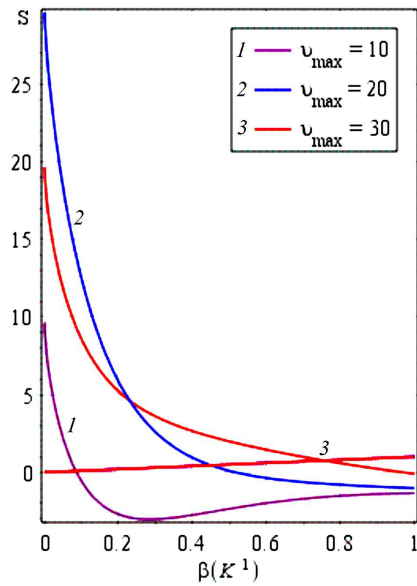


Fig. 13. Plot of free energy versus temperature at various v_{\max}

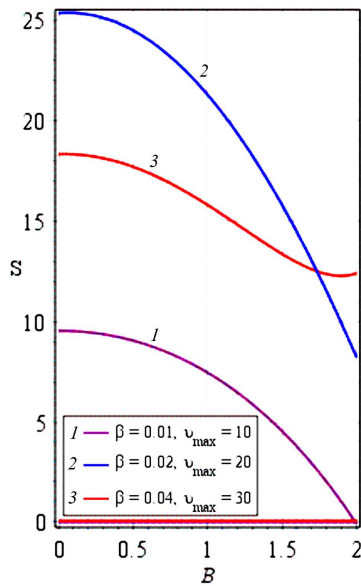


Fig. 14. Plot of free energy versus magnetic field at various temperatures and v_{\max}

is seen to behave itself differently. The mean energy decreases with increasing the AB flux.

The plot of the free energy against the temperature at various values of v_{\max} seen in Fig. 10 depicts an initial sharp increase of the free energy, but becomes invariant as the temperature increases. In Fig. 11, the

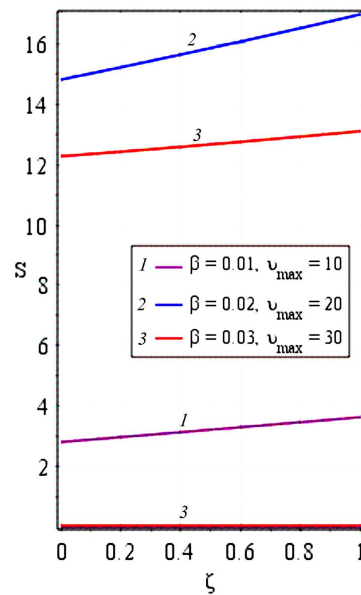


Fig. 15. Plot of entropy versus AB flux at different temperatures and v_{\max}

plot of the variation of free energy with increasing the magnetic field at various temperatures and v_{\max} can be seen. The free energy increases as the magnetic field intensifies. However, in Fig. 12, the free energy against the AB flux field shows that the free energy is seen to show a quasi-constant trend as the AB flux increases at various temperatures and v_{\max} . Figure 13 depicts the plot of the entropy with temperature variation at various v_{\max} . The entropy is observed to decrease monotonically as the temperature increases for $v_{\max} = 20$ and 30 ; but, for $v_{\max} = 10$, the entropy rose shortly and becomes fairly constant. Figure 14 is the entropy variation against the magnetic field at different temperatures and v_{\max} . The entropy is seen to decrease with the rise in the magnetic field strength. In Fig. 15, the plot of the entropy against the AB flux at different temperatures and v_{\max} shows that the entropy increases fairly with the rise in the AB flux field.

5. Conclusion

From our presented numerical results, we observe that, for the two different potential ranges of the potential well, the absence of both the magnetic field and the Aharonov Bohm (AB) flux, there were degeneracies in the energy levels of the system. However,

the application of both fields eliminated the degeneracies completely. We also noticed that the energy eigenvalues increase proportionally with the applications of both fields. That is, the trange δ is seen as a factor in sharpening the behavior of the energy eigenvalues. From our graphical plot of Figs. 1 and 2, we see that the energy eigenvalues increase proportionally as the magnetic field and AB flux fields are increasing. The partition function is calculated, and the thermodynamic properties such as the mean energy, free energy, and entropy are determined as functions of the temperature, magnetic and AB flux fields.

The authors wish to acknowledge the groups on theoretical physics at both Delta State University Abraka and the University of Port Harcourt, Rivers State, Nigeria.

The authors declare no conflict of interest.

1. H.K. Moghaddam, M.R. Maraki, A. Rajaei. Application of carbon nanotubes (CNT) on the computer science and electrical engineering: A review. *Inter. J. Reconfigurable and Embedded Systems (IJRES)* **9** (1), 61 (2020)
2. H.S.P. Wong and D Akinwande. Carbon nanotube and graphene device physics. *Contemp. Phys.* **53** (4), 1-1 (2012)
3. I.M. Ezeh, O.O.E. Enaroseha, G.K. Agbajor, F.I. Achuba. Effect of titanium oxide (TiO₂) on natural dyes for the fabrication of dye-sensitized solar cells. *Eng. Proc.* **63** (1), 25 (2024)
4. P.J.F. Harris, E. Hernández, B. Jakobson. Carbon nanotubes and related structure. New materials for the twenty-first. *American J. Phys.* **72** (3), 415 (2004)
5. I.S. Mosse, V.R. Sodisetti, C. Coleman, S. Ncube, A.S. de Sousa, R.M. Erasmus, E. Flahaut, T. Blon, B. Lassagne, T. Šamořil, S. Bhattacharyya. Tuning magnetic properties of a carbon nanotube-lanthanide hybrid molecular complex through controlled functionalization. *Molecule* **26** (3), 563 (2021)
6. L. Lindsay, D.A. Broido, N. Mingo. Flexural phonons and thermal transport in graphene. *Phys. Rev. B* **81** (11), 205441 (2010)
7. R.D. Folaron. *Manipulation of Carbon Nanotube Growth Direction Utilizing Magnetic Fields* (MSc Thesis, submitted to Rochester Institute of Technology, 2021)
8. V.N. Popov. Carbon nanotubes: Properties and application. *Material Sci. Eng. R Report* **43**, 61 (2004)
9. M.J. Biercuk, S. Ilani, C.M. Marcus, P.L. McEuen. Electrical Transport in Single-Wall Carbon Nanotubes. In *Carbon Nanotubes. Topics in Applied Physics*. Edited by A. Jorio, G. Dresselhaus, M.S. Dresselhaus. (Springer, 2007), Vol. 111.
10. S. Nanot, N.A. Thompson, K. Ji-Hee, X. Wang, W.D. Rice, C.L. Pint, J. Kono. Single-Walled Carbon Nanotube. In *Springer Handbook of Nanomaterials* (Springer-Verlag, 2013) [ISBN: 978-3-642-20594-1].
11. H. Hassanabadi, B.H. Yazarloo, S. Zarrinkamar, H. Rahimov. Deng–Fan potential for relativistic spinless particles – an ansatz solution. *Commun. Theor. Phys.* **57**, 339 (2012).
12. Z. Rang, H.G. Kjaergaard, M.L. Sage. Comparison of the morse and Deng–Fan potentials for xh bonds in small molecules. *Molecular Phys.* **101** (14), 2285 (2003).
13. C.A. Onate, O. Ebomwonyi, D.B. Olanrewaju. Application of Schrödinger equation in quantum well of Cu₂ZnSnS₄ quaternary semiconductor alloy. *Heliyon* **18** (6), e04062 (2020).
14. S.M. Ikhdair, Jamal Abu-Hasna. Quantization rule solution to the Hulthén potential in arbitrary dimension with a new approximate scheme for the centrifugal term. *Phys. Scripta* **83** (025002), 7 (2011).
15. C.O. Edet, P.O. Okoi, A.S. Yusuf, P.O. Ushie. Bound state solutions of the generalized shifted Hulthén potential. *Indian J. Phys.* **95**, 471 (2021).
16. A.N. Ikot, U.S. Okorie, P.O. Amadi, C.O. Edet, G.J. Rampho, R. Sever. The Nikiforov–Uvarov-Functional analysis (NUFA) method: A new approach for solving exponential-type potentials. *Few-Body Syst.* **62**, 9 (2021).
17. S.M. Ikhdair, B.J. Falaye, M. Hamzavi. nonrelativistic molecular models under external magnetic and AB flux fields. *Annals Phys.* **353**, 282 (2014).
18. I. Otete, C.B. Eleje. Magnetic field effect on the energy spectra of indium phosphide (InP) quantum dot in D-dimensions with the Hulthen–Yukawa potential. *Asian Res. J. Current Sci.* **5** (1), 20 (2023).
19. C.O. Zeinalipour-Yazdi, E.Z. Loizidou, A. Chutia. Size-dependent bond dissociation enthalpies in single-walled carbon nanotubes. *Chem. Phys. Lett.* **731**, 136628 (2019).
20. A.N. Ikot, U. Okorie, A.T. Ngiangia, C.A. Onate, C.O. Edet, I.O. Akpan, P.O. Amadi. Bound state solutions of the Schrödinger equation with energy-dependent molecular Kratzer potential via asymptotic iteration method. *Eclética Química J.* **45** (1), 65 (2020).
21. R. Khordad, H.R.R. Sedehi. Thermodynamic properties of a double ring-shaped quantum dot at low and high temperatures. *J. Low Temp. Phys.* **190**, 200 (2018).
22. U.O. Aigbe, R.B. Onyancha, K.E. Ukhurebor, B. Okundaye, E. Aigbe, Omamoke O.E. Enaroseha, K. Obodo, O.A. Osibote, A. El Nemr, L.L. Noto, Harrison I. Atagana. Utility of Magnetic Nanomaterials for Theranostic Nanomedicine. In: *Magnetic Nanomaterials: Synthesis, Characterization and Applications*. Edited by U.O. Aigbe, K.E. Ukhurebor, R.B. Onyancha (Springer Nature, 2023).

23. G.I. Okunzuwa, Omamoke O.E. Enaroseha, S. Okunzuwa. Synthesis and characterization of Fe(III) chitosan nanoparticles n-benzaldehyde schiff base for biomedical application. *Chem. Pap.* **78** (5) 3258 (2024). Received 16.02.24

*I. Otete, O.O.E. Enaroseha,
S.I. Rkumzuwa, A.I.I. Edjere*

СПЕКТРИ ТА ТЕРМОДИНАМІЧНІ
ВЛАСТИВОСТІ ЗИГЗАГОПОДІБНИХ ОДНОСТІННИХ
ВУГЛЕЦЕВИХ НАНОТРУБОК З ПОТЕНЦІАЛОМ
ДЕНГА–ФАНА–ХЮЛЬТЕНА

Виконано теоретичне дослідження спектрів та термодинамічних властивостей зигзагоподібних одностінних вуглеце-

вих нанотрубок (6,0) з потенціалом Денга–Фана–Хюльтена. Знайдено аналітичний розв'язок рівняння Шрьодінгера за допомогою методу Нікіфорова–Уварова для системи в присутності магнітного поля і поля Ааронова–Бома. Розраховано статистичну суму і залежності термодинамічних величин системи від полів та температури.

Ключові слова: потенціал Денга–Фана–Хюльтена, магнітне поле, поле Ааронова–Бома, метод Нікіфорова–Уварова.